

# SAR Image Synthesis with Diffusion Models

Denisa Qosja, Simon Wagner, Daniel O’Hagan  
Fraunhofer Institute for High Frequency Physics and Radar Techniques FHR  
{denisa.qosja, simon.wagner, daniel.ohagan}@fhr.fraunhofer.de

**Abstract**—In recent years, diffusion models (DMs) have become a popular method for generating synthetic data. By achieving samples of higher quality, they quickly became superior to generative adversarial networks (GANs) and the current state-of-the-art method in generative modeling. However, their potential has not yet been exploited in radar, where the lack of available training data is a long-standing problem. In this work, a specific type of DMs, namely denoising diffusion probabilistic model (DDPM) is adapted to the SAR domain. We investigate the network choice and specific diffusion parameters for conditional and unconditional SAR image generation. In our experiments, we show that DDPM qualitatively and quantitatively outperforms state-of-the-art GAN-based methods for SAR image generation. Finally, we show that DDPM profits from pretraining on large-scale clutter data, generating SAR images of even higher quality.

**Index Terms**—Denoising Diffusion Probabilistic Model (DDPM), Generative Adversarial Networks (GANs), synthetic aperture radar (SAR), synthetic data

## I. INTRODUCTION

Synthetic Aperture Radar (SAR) technology provides high-resolution imaging data used in various applications such as surveillance, defense, remote sensing, among others. Clear images, regardless of light and weather conditions, are benefits that make SAR such a valuable sensor. However, it comes with high costs of acquisition, which makes the availability of data scarce. That sets off a problem in the era of deep learning, where training neural networks requires large-scale datasets in order to appropriately extract information from the data while maintaining an adequate generalization. Target recognition with SAR [1], [2] is therefore limited and advances at a slow pace relative to advances in comparable fields, such as LiDAR.

To overcome the lack of abundant radar training data, efforts have been made to obtain synthetically generated data. SAR simulators have been developed through the years to simulate either images directly from real input data [3]–[6] or from raw signals [7]–[11], from which the images are obtained after raw data processing. The major benefit of simulations is the reduced acquisition costs for the data, but also the reduced cost, time and effort in obtaining annotations, overcoming the need of manual labelling. However, there are downsides to using only simulated data. The simulators are usually specified to represent targets in a specific background, e.g. sea, earth or forests, and different simulators have to be developed in order to portray different environments. Furthermore, they do not

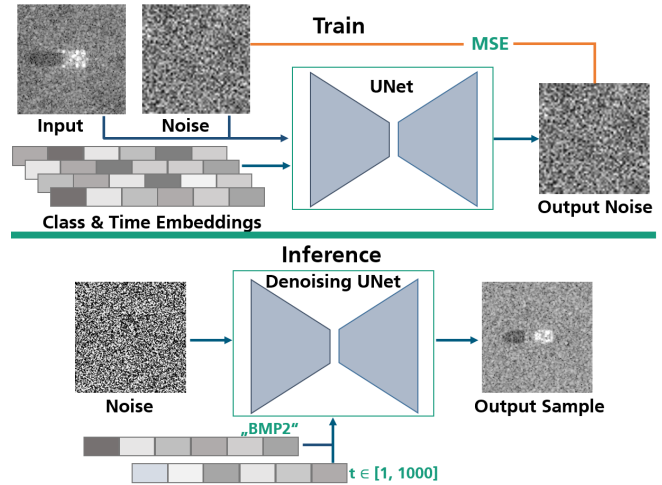


Fig. 1: Training and inference phases for DDPM. During training, input SAR data infused with noise, timestep and class embeddings are fed to the UNet model, which learns to predict the noise added to the input samples. During inference, noise is sampled from a normal distribution, fed to the UNet and iteratively denoised to finally obtain a SAR image.

represent the full spectrum of the real-case scenario clutter, creating datasets that are far from the realism of the world.

Generative modeling with neural networks, which has shown promise to synthesize novel SAR samples, could overcome the limitations of simulators. Generative Adversarial Networks (GANs) [12] have been for a long time the state-of-the-art network in the field and continue to be developed to achieve data of high realism and fidelity. In radar, they have already been used for various purposes. In [13], an end-to-end GAN has been employed to generate 1000 samples for each class of MSTAR dataset. They make a clear analysis of why the clutter and speckle influence the network towards mode collapse and propose a normalization method to stabilize and accelerate the training process. More sophisticated versions of GANs, such as conditional GAN, WGAN, BEGAN, etc [14]–[16] have been investigated and developed to generate synthetic samples. In addition, an extensive work has been made towards image translation [17], [18] in order to convert samples from SAR to the optical domain. GANs have been used to modify the simulated data by augmentations [19] and then using it as the training set for automatic target recognition (ATR) [20], [21]. Despite these recent advances in applying GANs to SAR data, training GANs still remains a challenging

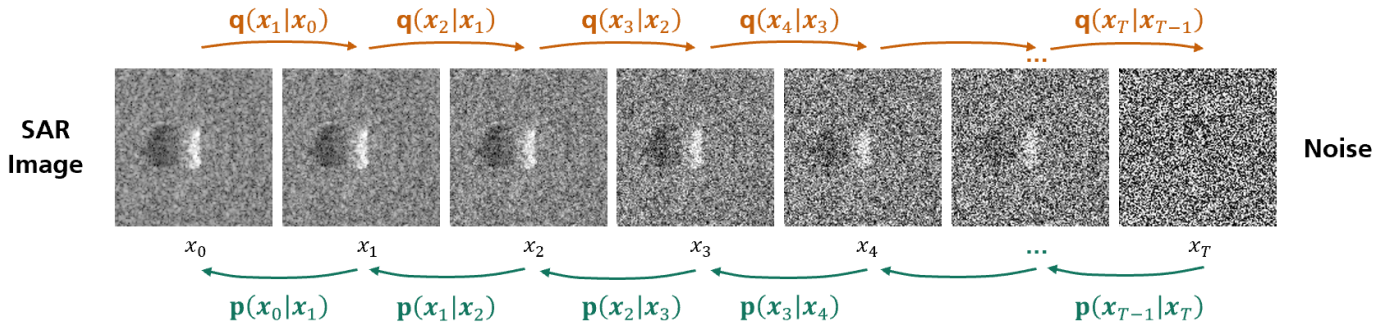


Fig. 2: DDPM processing illustrated with the MSTAR dataset. The model is comprised of two processes: a **forward diffusion process** that adds noise to the data and learns it for each timestep  $t$ ; and a **reverse denoising process** that draws samples from a Gaussian noise at time  $T$  and iteratively denoises its input to generate new data samples.

task due to training instability, low diversity, mode collapse and difficult hyperparameter optimization [22].

In the recent years, diffusion models [23] have emerged as a potential method in generating high quality data. They have quickly achieved state-of-the-art results in the vision field by surpassing GANs. In the radar field, however these networks have not yet found a broad application except for a recent work in the SAR domain where speckle is removed from the data [24].

In this paper, we investigate Denoising Diffusion Probabilistic Models (DDPM) [25] to generate SAR data. An overview of our proposed approach is shown in Fig. 1. Firstly, we describe the fundamentals of DDPM and discuss different design choices and parameters to adapt them to the SAR domain. We train DDPM on the MSTAR [26] dataset in order to generate a large number of novel samples. With the goal of extending the amount of available labelled data, we feed the network with class information in order to generate accurate images conditioned on the given category. Nonetheless, both class-conditional and unconditional versions of DDPM are evaluated and compared with GANs. Additionally, we show that by pretraining DDPM on a large-scale dataset of clutter images and fine-tuning it on MSTAR targets, we can generate SAR images of even higher quality.

Whereas most previous works on SAR image generation seldom report quantitative metrics, in this work, we benchmark DDPM and different GAN-based models using three popular evaluation metrics, namely Inception Score (IS) [27], Fréchet Inception Distance (FID) [28] and Kernel Inception Distance (KID) [29]. We qualitative and quantitative show that DDPM synthesizes MSTAR targets significantly more accurately and with higher fidelity than GANs.

In section II, the DDPM will be revised, followed by a description of the method used to generate SAR data and the metrics used to evaluate them in section III. Experimental results from various networks and comparisons among them are described in section IV. Finally, the paper is concluded in section V.

## II. DENOISING DIFFUSION PROBABILISTIC MODELS

DDPM was introduced by Ho et al. [25]. DDPM is composed of a Markov chain, known as a forward diffusion process, where the data is infused gradually with Gaussian noise. It is followed by a reverse denoising process, with the learned noise being removed to generate a new data sample which has the same distribution as the original data. The simple idea of DDPM is displayed in Fig. 2.

### A. Forward Diffusion Process

Suppose that a training sample  $\mathbf{x}_0$  is of certain distribution, denoted as  $q(\mathbf{x}_0)$ . In the forward diffusion process, Gaussian noise with variance  $\beta_t \in (0, 1)$  is added gradually to the sample  $\mathbf{x}_0$  for  $T$  steps. The number of timesteps  $T$  is chosen to be large enough so that a latent sample  $\mathbf{x}_T$  with isotropic Gaussian distribution is obtained:  $\mathbf{x}_T \sim \mathcal{N}(0, \mathbf{I})$ .

The posterior distribution, which transitions into latent space to provide samples injected with Gaussian noise  $\mathbf{x}_1, \dots, \mathbf{x}_T$ , is defined as:

$$q(\mathbf{x}_{1:T}|\mathbf{x}_0) = \prod_{t=1}^T q(\mathbf{x}_t|\mathbf{x}_{t-1}), \quad (1)$$

$$q(\mathbf{x}_t|\mathbf{x}_{t-1}) := \mathcal{N}(\mathbf{x}_t, \sqrt{1 - \beta_t}\mathbf{x}_{t-1}, \beta_t\mathbf{I}). \quad (2)$$

To make the forward process faster, the samples  $\mathbf{x}_t$  can be sampled arbitrarily at any timestep  $t$ . Using the notations  $\alpha_t := 1 - \beta_t$  and  $\bar{\alpha}_t := \prod_{s=1}^t \alpha_s$ , the posterior probability can be rewritten as

$$q(\mathbf{x}_t|\mathbf{x}_0) = \mathcal{N}(\mathbf{x}_t, \sqrt{\alpha_t}\mathbf{x}_0, (1 - \bar{\alpha}_t)\mathbf{I}). \quad (3)$$

The posterior  $q$  has no learnable parameters which makes the forward process fixed (the variances  $\beta_t = 1 - \bar{\alpha}_t$  are not learnable). Therefore, the sample  $\mathbf{x}_t$  can be defined directly as

$$\mathbf{x}_t = \sqrt{\alpha_t}\mathbf{x}_0 + \sqrt{1 - \bar{\alpha}_t}\boldsymbol{\epsilon}, \quad \boldsymbol{\epsilon} \sim \mathcal{N}(0, \mathbf{I}). \quad (4)$$

## B. Reverse Denoising Process

The reverse denoising process aims to sample reversely from  $\mathbf{x}_T$  through transition probabilities  $q(\mathbf{x}_{t-1}|\mathbf{x}_t)$  for timesteps  $T - 1$  through 1 to obtain a sample drawn from  $q(\mathbf{x})$ . The transition  $q(\mathbf{x}_{t-1}|\mathbf{x}_t)$  is a Gaussian distribution, tractable when conditioned on  $\mathbf{x}_0$ , defined as:

$$q(\mathbf{x}_{t-1}|\mathbf{x}_t, \mathbf{x}_0) = \mathcal{N}(\mathbf{x}_{t-1}, \tilde{\boldsymbol{\mu}}_t(\mathbf{x}_t, \mathbf{x}_0), \tilde{\beta}_t \mathbf{I}). \quad (5)$$

As shown in [30], using Bayes' rule, the mean  $\tilde{\boldsymbol{\mu}}_t$  and variance  $\tilde{\beta}_t$  are calculated to be:

$$\sigma_t^2 = \tilde{\beta}_t = \frac{1 - \bar{\alpha}_{t-1}}{1 - \bar{\alpha}_t} \beta_t, \quad (6)$$

$$\tilde{\boldsymbol{\mu}}_t(\mathbf{x}_t, \mathbf{x}_0) := \frac{\sqrt{\bar{\alpha}_{t-1}} \beta_t}{1 - \bar{\alpha}_t} \mathbf{x}_0 + \frac{\sqrt{\alpha_t} (1 - \bar{\alpha}_{t-1})}{1 - \bar{\alpha}_t} \mathbf{x}_t. \quad (7)$$

Replacing  $\mathbf{x}_0$  from (4):

$$\tilde{\boldsymbol{\mu}}_t(\mathbf{x}_t, \mathbf{x}_0) = \frac{1}{\sqrt{\alpha_t}} \left( \mathbf{x}_t - \frac{1 - \alpha_t}{\sqrt{1 - \bar{\alpha}_t}} \boldsymbol{\epsilon}_t \right). \quad (8)$$

Given that the estimation of the reverse transition probability  $p_\theta(\mathbf{x}_{t-1}|\mathbf{x}_t)$  relies on the entire data distribution, it can be approximated through a neural network:

$$p_\theta(\mathbf{x}_{t-1}|\mathbf{x}_t) = \mathcal{N}(\mathbf{x}_{t-1}, \boldsymbol{\mu}_\theta(\mathbf{x}_t, t), \boldsymbol{\Sigma}_\theta(\mathbf{x}_t, t)), \quad (9)$$

where, following [25],  $\boldsymbol{\Sigma}_\theta(\mathbf{x}_t, t) = \tilde{\beta}_t \mathbf{I}$  is a fixed variance, and the mean  $\boldsymbol{\mu}_\theta(\mathbf{x}_t, t)$  depends on a noise sample  $\boldsymbol{\epsilon}_\theta(\mathbf{x}_t, t)$  which is learned by a neural network, conditioned on the current sample  $\mathbf{x}_t$  and timestep  $t$ . The learning process is guided by the objective function

$$L = \mathbb{E}_{t, \mathbf{x}_0, \boldsymbol{\epsilon}} [ \|\boldsymbol{\epsilon} - \boldsymbol{\epsilon}_\theta(\mathbf{x}_t, t)\|^2 ], \quad (10)$$

while the output sample is obtained as follows:

$$\begin{aligned} \mathbf{x}_{t-1} &= \boldsymbol{\mu}_\theta(\mathbf{x}_t, t) + \sigma_t \mathbf{z}, \\ &= \frac{1}{\sqrt{\alpha_t}} \left( \mathbf{x}_t - \frac{1 - \alpha_t}{\sqrt{1 - \bar{\alpha}_t}} \boldsymbol{\epsilon}_\theta(\mathbf{x}_t, t) \right) + \sigma_t \mathbf{z}. \end{aligned} \quad (11)$$

$$\begin{cases} \mathbf{z} \sim \mathcal{N}(0, \mathbf{I}), & \text{if } t > 1 \\ \mathbf{z} = 0, & \text{otherwise.} \end{cases} \quad (12)$$

## C. Design Choices

To decide on the design of the network, we rely mostly on the original work by Ho et al. [25].

**Diffusion Steps:**  $T$  is chosen to be sufficiently large, namely  $T = 1000$  in order to obtain a sample  $\mathbf{x}_T$  with an isotropic Gaussian distribution.

**Noise Schedule:** The noise is added to the input data in a linear manner, however it is argued in [31] that it does not contribute much towards the end of the diffusion process. In this work, we explore two other schedulers, namely cosine and sigmoid, with variances as shown in Fig. 3. Based on our experiments, the linear manner of infusing noise performs the best in SAR. We argue that the quick decay of the noise levels occurring in early time steps in the linear scheduler leads to an improved performance.

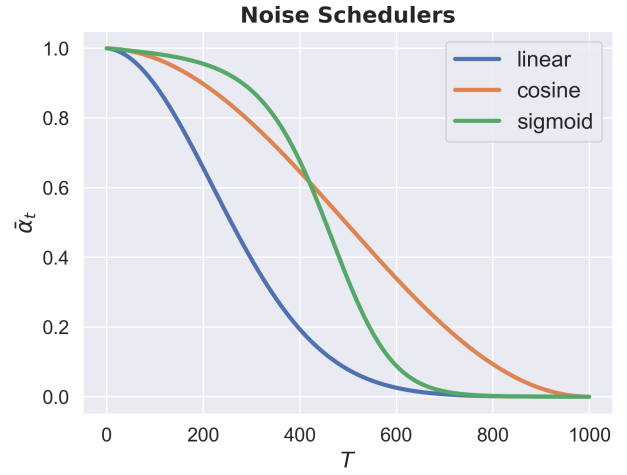


Fig. 3: The behaviour of  $\bar{\alpha}_t$  for different noise schedulers.

**$\beta$  Range:** The variance range is decided to be in between  $\beta_1 = 10^{-4}$  and  $\beta_T = 0.02$ , considering that data has to be scaled to  $[-1, 1]$  before being fed to the network.

**Conditional DDPM:** Conditional generative models are designed to generate data based on condition presented to them. Since targets from certain classes are desired, the condition is simply the class information embedded into each downsampling and upsampling block of the network.

## D. Model - UNet

The model used to learn the Gaussian noise added to the data samples is a UNet [32] composed of eight residual blocks in the compression and in the extension side, with three downsampling and upsampling layers respectively. The network is equipped with residual connections to fight vanishing gradients and skip connections to recover high detailed information at the extension part.

Following [25], the network includes group normalization layers [33], self-attention blocks at  $32 \times 32$  feature map resolution, a dropout layer with  $p = 0.3$ , time and label embeddings, and Swish activation function [34].

## III. SAR DATA GENERATION

In this work, we make use of MSTAR dataset which is composed of a training set with 2693 images and a test set with 4357 images. We aim to extend the training set by generating 10k synthetic samples. Before being fed to the network, the data should be normalized to range  $[-1, 1]$ .

### A. MSTAR Clutter

Since the scale of the MSTAR dataset is small, we propose to exploit the larger amount of unlabelled clutter images for pretraining generative models.

We employ the MSTAR clutter data, which includes large scenarios of the environment where MSTAR targets were acquired. Scenes like trees, fields and roads are depicted in 100 images of large sizes, mostly  $1784 \times 1476$ . These images are preprocessed into same shapes as MSTAR targets

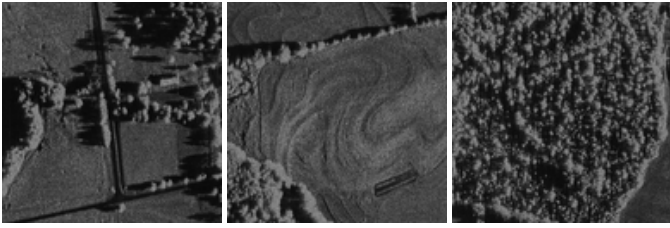


Fig. 4: The clutter data depicts the surroundings of MSTAR targets, and illustrates scenarios such as fields, trees and roads.

of  $128 \times 128$ , and converted into logarithmic scale, resulting in 14.3k training samples. Examples of unprocessed clutter data are shown in Fig. 4.

With the goal of generating higher quality images, we propose to first pretrain generative models on the MSTAR clutter dataset, and then fine-tune them on MSTAR targets for class-conditional image generation.

### B. GANs Architectures

We compare DDPM with three popular GAN variants which have shown success for synthesising MSTAR images; namely Deep Convolutional GAN (DCGAN) [35], Self-Attention GAN (SAGAN) [36] and Wasserstein GAN (WGAN) [37].

DCGAN is the first version of GANs to introduce strided convolutional layers in the architecture. It enforced the usage of batch normalization stabilizing the training, and proposed leaky ReLU as the activation function at the discriminator while maintaining ReLU at the generator.

SAGAN introduced a self-attention mechanism in convolutional GANs to model long-range dependencies across image regions. In addition, it comes with some different design choices, such as spectral normalization [38], class conditioning inside the batch normalization layer at the generator, and the hinge version of the adversarial loss. Other changes include using different learning rates for the generator and discriminator.

WGAN was introduced as a version of GANs which uses the Wasserstein’s distance as the loss function and improves the mode collapse issue. In this work, we combine the SAGAN architecture with the Wasserstein’s loss. In addition, we use gradient penalty instead of weight clipping.

### C. Evaluation Protocol

When measuring the performance of a generative model, two characteristics of the synthetic data should be considered: fidelity and diversity. It is important that the fake samples are of high quality and as close as possible to the real data, and that the generated set is of high diversity, covering the distribution of the real set.

Since a standardized evaluation protocol has not yet been established in SAR image generation, we define the following evaluation pipeline. Given a generative model (i.e. DDPM or GAN) trained on MSTAR, we generate 10k novel samples, and evaluate them using the IS, FID and KID metrics, which employ an InceptionNetV3 [39] pretrained on MSTAR.

TABLE I: Evaluation of unconditional (top) and conditional (bottom) GANs and DDPM. DDPM clearly outperforms GAN-based models.

Model	IS $\uparrow$	FID $\downarrow$	KID $\downarrow$
DCGAN [35]	4.19	7.10	0.0053
SAGAN [36]	7.00	3.11	0.0025
DDPM [25]	<b>8.64</b>	<b>0.77</b>	<b>0.0004</b>
cDCGAN [35]	7.60	3.60	0.0035
cSAGAN [36]	9.39	2.46	0.0017
cWGAN [37]	7.00	1.59	0.0008
cDDPM [25]	<b>9.77</b>	<b>0.38</b>	<b>0.0003</b>

IS uses a pretrained InceptionNetV3 to predict conditional probabilities of the generated samples. A high classification value implies a sample with high quality. The diversity is measured as the Kullback-Leibler (KL) divergence between the marginal and conditional probability distributions. Both outcomes are combined into scores that show good results from the generative network. A large combination of both outcomes indicates generated samples of high quality and diversity. However, the IS does not consider the statistics of the real data and also does not measure the intra-class diversity.

FID was developed to improve on the drawbacks of the IS. The InceptionNetV3 extracts features of dimensionality 2048 from both real and fake data, which are then embedded into multivariate Gaussian distributions. Fréchet distance outputs a similarity score in the distribution between measured data and generated one. The smaller the score, the closer the distribution is. However, the statistics to calculate the distance (mean and variance) make the FID dependent on the data size.

KID overcomes the data size issue, by calculating the maximum mean discrepancy between features of the real and generated data.

## IV. EXPERIMENTS

In this section, we evaluate the performance of DDPM and compare it to the GAN variants. All networks are trained both for conditional and unconditional SAR image generation for 200 epochs, using a batch size of 32. DDPM has an initial channel size 64 which doubles at each downsampling step. For all GANs, this initial value is set to 16. The pretraining on clutter data is set for 500 epochs, followed by 200 epochs of fine-tuning on MSTAR for class-conditional generation. These parameters are chosen through empirical validation.

In Fig. 5, a few samples from all class-conditioned architectures are shown. The images in each row belong to the classes M548, M35 (x2), 2S1 and BTR70 from left to right. The synthetic data obtained by DCGAN includes visible artifacts, unclear target shapes and ring-like patterns around the targets. The quality in SAGAN-generated data is improved, but similarly to WGAN, they still lack high fidelity. Most of the artifacts present in GAN-generated samples are resolved by DDPM, which can also represent more accurately reflections.

Quantitative results in terms of IS, FID and KID are given in Table I, where best achieved results are in bold. On the top

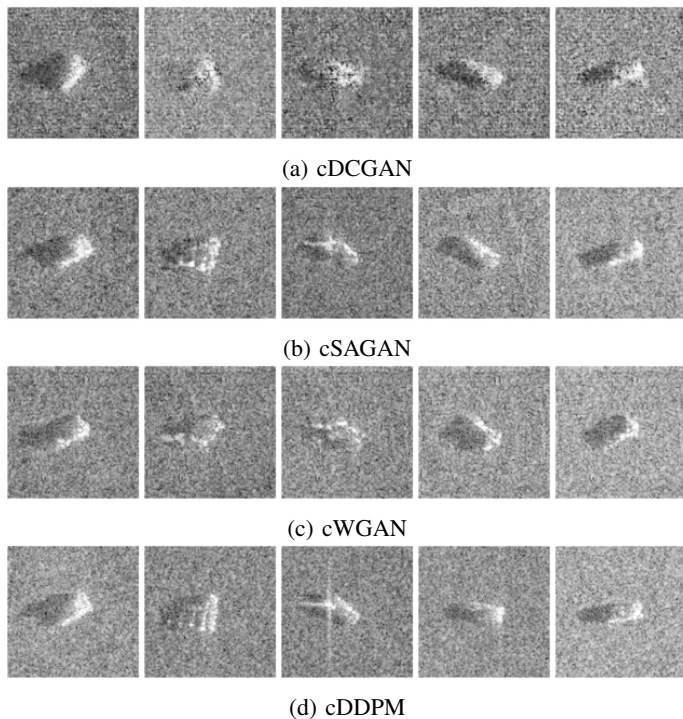


Fig. 5: Images generated by class-conditioned generative networks. The images generated by cDDPM represent the background in a more accurate way and reconstruct the targets more precisely.

TABLE II: Evaluation of pretrained GANs and DDPM.

	Model	IS $\uparrow$	FID $\downarrow$	KID $\downarrow$
cDCGAN [35]	no pretraining	<b>7.60</b>	<b>3.60</b>	<b>0.0035</b>
	pretraining	3.87	9.93	0.0060
cDDPM [25]	no pretraining	<b>9.77</b>	0.38	0.0003
	pretraining	9.74	<b>0.23</b>	<b>0.0001</b>

part, the values are obtained from the unconditional architectures, while on the bottom from their conditional counterpart. As expected, the conditional versions improve the quality and diversity of the data with respect to the unconditional ones. In both cases, DDPM achieves the best performance with a significant improvement with respect to the GAN architectures.

For a closer look on the performance of DDPM in SAR, in Fig. 6, generated MSTAR images of categories M1, T72 and BTR70 are shown alongside ground truth samples from the corresponding class. We show that DDPM is able to synthesize high diversity data from various azimuth angles. DDPM generates high quality images with target shapes reconstructed accurately and background represented adequately.

In Table II, we compare DCGAN and DDPM models first pretrained with clutter background and then fine-tuned on MSTAR, with their unpretrained counterparts. Whereas clutter pretraining deteriorates the results for DCGAN, DDPM highly benefits from the pretraining, showing superior quantitative

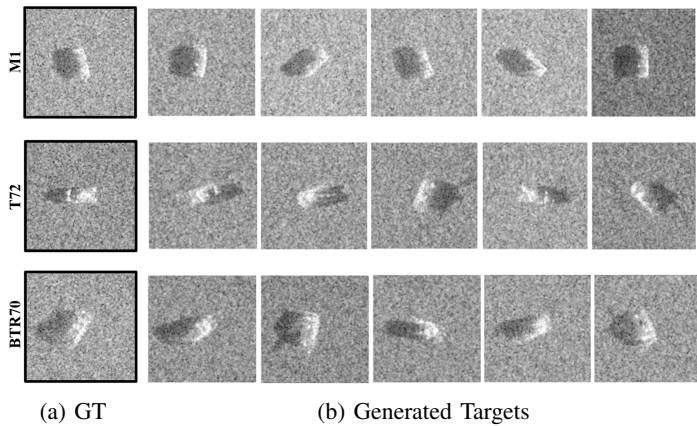


Fig. 6: (a) Ground truth MSTAR images of classes M1, T72 and BTR70. (b) Synthetic samples generated by DDPM when conditioned on the corresponding class.

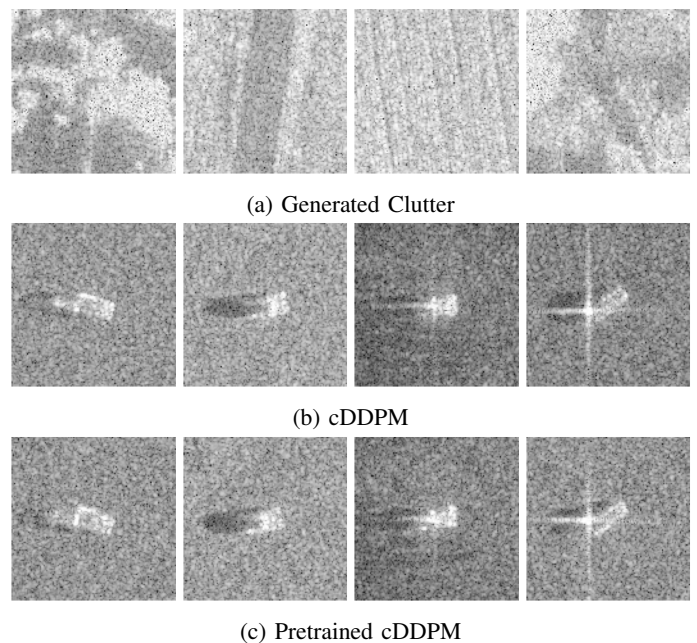


Fig. 7: (a) Clutter generated during pretraining by DDPM. (b) Targets generated by unpretrained conditional DDPM. (c) Targets generated by DDPM pretrained on clutter and fine-tuned on MSTAR for conditional image generation.

performance. Fig. 7a depicts images of clutter generated by DDPM during pretraining. We can clearly distinguish different clutter scenarios, such as trees, fields and roads. Fig 7b and 7c show images generated by the unpretrained and pretrained DDPM, respectively, using the same class condition. Despite the superior quantitative performance achieved by pretraining, both models generate realistic SAR samples.

## V. CONCLUSIONS

In this work, the diffusion models are brought to the SAR domain for the purpose of image synthesis. We showed that DDPM quantitatively outperforms GAN-based models on the MSTAR dataset on three evaluation metrics, while

generating samples of higher quality. Additionally, we showed that DDPM can leverage large amounts of unlabelled clutter data for pretraining, leading to higher quality results. As future work, we aim to use our high quality synthetic data to extend the small-scale available datasets for downstream tasks, such as target classification and detection. Furthermore, we plan to explore DDPM for other imaging tasks, such as image translation and super-resolution.

## REFERENCES

- [1] S. A. Wagner, "SAR ATR by a Combination of Convolutional Neural Network and Support Vector Machines," *IEEE Transactions on Aerospace and Electronic Systems*, 2016.
- [2] D. Qosja, S. Wagner, and S. Brüggewirth, "Benchmarking Convolutional Neural Network Backbones for Target Classification in SAR," in *2023 IEEE Radar Conference (RadarConf23)*, 2023.
- [3] M. L. Williams, "PolSARproSim - A Coherent Polimetric SAR Simulation of Forests for PolSARproSim," *European Space Agency*, 2006.
- [4] S. Auer, R. Bamler, and P. Reinartz, "RaySAR-3D SAR Simulator: Now Open Source," in *IEEE International Geoscience and Remote Sensing Symposium (IGARSS)*. IEEE, 2016, pp. 6730–6733.
- [5] H. Hammer and K. Schulz, "Coherent Simulation of SAR Images." International Society for Optics and Photonics, 2009.
- [6] C. Cochin, P. Pouliguen, B. Delahaye, D. le Hellard, P. Gosselin, and F. Aubineau, "MOCEM-An'all in one'tool to simulate SAR image," in *7th European Conference on Synthetic Aperture Radar*, 2008.
- [7] G. Franceschetti, M. Migliaccio, and D. Riccio, "The SAR Simulation: An Overview," in *International Geoscience and Remote Sensing Symposium*, 1995.
- [8] G. Franceschetti, M. Migliaccio, D. Riccio, and G. Schirrinzi, "SARAS: A Synthetic Aperture Radar(SAR) Raw Signal Simulator," *IEEE Transactions on Geoscience and Remote Sensing*, 1992.
- [9] A. Mori and F. De Vita, "A Time-Domain Raw signal Simulator for Interferometric SAR," *IEEE Transactions on Geoscience and Remote Sensing*, 2004.
- [10] G. Margarit, J. J. Mallorqui, J. M. Rius, and J. Sanz-Marcos, "On the Usage of GRECOSAR, an Orbital Polarimetric SAR Simulator of Complex Targets, to Vessel Classification Studies," *IEEE Transactions on Geoscience and Remote Sensing*, 2006.
- [11] J. Drozdowicz, "The Open-Source Framework for 3D Synthetic Aperture Radar Simulation," *IEEE Access*, 2021.
- [12] I. Goodfellow, J. Pouget-Abadie, M. Mirza, B. Xu, D. Warde-Farley, S. Ozair, A. Courville, and Y. Bengio, "Generative Adversarial Nets," *Advances in neural information processing systems*, 2014.
- [13] J. Guo, B. Lei, C. Ding, and Y. Zhang, "Synthetic Aperture Radar Image Synthesis by using Generative Adversarial Nets," *IEEE Geoscience and Remote Sensing Letters*, 2017.
- [14] J. Qin, Z. Liu, L. Ran, R. Xie, J. Tang, and Z. Guo, "A Target SAR Image Expansion Method Based on Conditional Wasserstein Deep Convolutional GAN for Automatic Target Recognition," *IEEE Journal of Selected Topics in Applied Earth Observations and Remote Sensing*, 2022.
- [15] Z. Luo, X. Jiang, and X. Liu, "Synthetic Minority Class Data by Generative Adversarial Network for Imbalanced SAR Target Recognition," in *IEEE International Geoscience and Remote Sensing Symposium IGARSS*. IEEE, 2020.
- [16] X. Liu, Y. Huang, C. Wang, J. Pei, W. Huo, Y. Zhang, and J. Yang, "Semi-Supervised SAR ATR via Conditional Generative Adversarial Network with Multi-Discriminator," in *IEEE International Geoscience and Remote Sensing Symposium IGARSS*, 2021.
- [17] M. Fuentes Reyes, S. Auer, N. Merkle, C. Henry, and M. Schmitt, "SAR-to-Optical Image Translation Based on Conditional Generative Adversarial Networks—Optimization, Opportunities and Limits," *Remote Sensing*, 2019.
- [18] Z. Zuo and Y. Li, "A SAR-to-Optical Image Translation Method Based on PIX2PIX," in *IEEE International Geoscience and Remote Sensing Symposium IGARSS*, 2021.
- [19] J. Hwang and Y. Shin, "Image Data Augmentation for SAR Automatic Target Recognition Using TripleGAN," in *2021 International Conference on Information and Communication Technology Convergence (ICTC)*, 2021.
- [20] Z. Cui, M. Zhang, Z. Cao, and C. Cao, "Image Data Augmentation for SAR Sensor via Generative Adversarial Nets," 2019.
- [21] B. Camus, E. Monteux, and M. Vermet, "Refining Simulated SAR Images with Conditional GAN to Train ATR algorithms," in *Actes de la conférence CAID*, 2020.
- [22] D. Saxena and J. Cao, "Generative Adversarial Networks (GANs) Challenges, Solutions, and Future Directions," *ACM Computing Surveys (CSUR)*, 2021.
- [23] J. Sohl-Dickstein, E. Weiss, N. Maheswaranathan, and S. Ganguli, "Deep Unsupervised Learning using Nonequilibrium Thermodynamics," in *International Conference on Machine Learning (PMLR)*, 2015.
- [24] M. V. Perera, N. G. Nair, W. G. C. Bandara, and V. M. Patel, "SAR Despeckling using a Denoising Diffusion Probabilistic Model," *IEEE Geoscience and Remote Sensing Letters*, 2023.
- [25] J. Ho, A. Jain, and P. Abbeel, "Denoising Diffusion Probabilistic Models," *Advances in Neural Information Processing Systems (NeurIPS)*, 2020.
- [26] E. R. Keydel, S. W. Lee, and J. T. Moore, "MSTAR Extended Operating Conditions: A Tutorial." International Society for Optics and Photonics, 1996.
- [27] T. Salimans, I. Goodfellow, W. Zaremba, V. Cheung, A. Radford, and X. Chen, "Improved Techniques for Training GANs," *Advances in Neural Information Processing Systems (NeurIPS)*, 2016.
- [28] M. Heusel, H. Ramsauer, T. Unterthiner, B. Nessler, and S. Hochreiter, "Gans Trained by a Two Time-Scale Update Rule Converge to a Local Nash Equilibrium," *Advances in neural information processing systems*, 2017.
- [29] M. Bińkowski, D. J. Sutherland, M. Arbel, and A. Gretton, "Demystifying MMD GANs," *arXiv preprint arXiv:1801.01401*, 2018.
- [30] L. Weng, "What are diffusion models?" *lilianweng.github.io*, 2021.
- [31] A. Q. Nichol and P. Dhariwal, "Improved Denoising Diffusion Probabilistic Models," in *International Conference on Machine Learning*, 2021.
- [32] O. Ronneberger, P. Fischer, and T. Brox, "U-Net: Convolutional Networks for Biomedical Image Segmentation," in *Medical Image Computing and Computer-Assisted Intervention—MICCAI*, 2015.
- [33] Y. Wu and K. He, "Group Normalization," in *Proceedings of the European conference on computer vision (ECCV)*, 2018.
- [34] P. Ramachandran, B. Zoph, and Q. V. Le, "Searching for Activation Functions," *arXiv preprint arXiv:1710.05941*, 2017.
- [35] A. Radford, L. Metz, and S. Chintala, "Unsupervised Representation Learning with Deep Convolutional Generative Adversarial Networks," *arXiv preprint arXiv:1511.06434*, 2015.
- [36] H. Zhang, I. Goodfellow, D. Metaxas, and A. Odena, "Self-Attention Generative Adversarial Networks," in *International Conference on Machine Learning*. PMLR, 2019.
- [37] M. Arjovsky, S. Chintala, and L. Bottou, "Wasserstein Generative Adversarial Networks," in *International conference on machine learning*. PMLR, 2017.
- [38] T. Miyato, T. Kataoka, M. Koyama, and Y. Yoshida, "Spectral Normalization for Generative Adversarial Networks," *International Conference on Learning Representations (ICLR)*, 2018.
- [39] C. Szegedy, W. Liu, Y. Jia, P. Sermanet, S. Reed, D. Anguelov, D. Erhan, V. Vanhoucke, and A. Rabinovich, "Going Deeper with Convolutions," in *Proceedings of the IEEE Conference on Computer Vision and Pattern Recognition (CVPR)*, 2015.